# Probing Metal−Support Interactions under Oxidizing and Reducing Conditions: In Situ Raman and Infrared Spectroscopic and Scanning Transmission Electron Microscopic−X-ray Energy-Dispersive Spectroscopic Investigation of Supported Platinum Catalysts

**Wenyong Lin,[†] A. A. Herzing,[‡] C. J. Kiely,[‡] and I. E. Wachs*,[†]**

*Operando Molecular Spectroscopy and Catalysis Laboratory, Chemical Engineering Department, Center for Advanced Materials and Nanocharacterization, and Materials Science & Engineering Department, Lehigh University, Bethlehem, Pennsylvania 18015*

*Received: November 4, 2007; In Final Form: January 16, 2008*

The strength of PtOx−support and Pt−support interactions was investigated for supported PtOx/$SiO_2$, PtOx/$Al_2O_3$, and PtOx/$CeO_2$ catalysts with time-resolved in situ Raman/IR spectroscopy and scanning transmission electron microscopy (STEM). Raman spectroscopy (and STEM−X-ray energy-dispersive spectoscopy, XEDS) was able to distinguish between crystalline $PtO_2$ (4−7 nm), amorphous $PtO_2$ (∼1−1.5 nm), and surface PtOx species (<1 nm). The domain size of the supported PtOx phase decreased ($SiO_2$ > $Al_2O_3$ > $CeO_2$) as the PtOx−support interaction increased ($CeO_2$ > $Al_2O_3$ > $SiO_2$). The strength of the PtOx−support interaction also controlled the reducibility of the supported PtOx phase, with the strongly interacting PtOx/$CeO_2$ system being the most difficult to reduce. Corresponding IR spectroscopy showed that the $CeO_2$ support also became reduced by H-spillover during the reduction treatment. Furthermore, Pt redispersion is also related to the PtOx−support interaction, and complete redispersion on $CeO_2$ can be achieved with mild reduction−oxidation treatments. The reduced metallic Pt is reoxidized by bulk lattice oxygen from the $CeO_2$ support and not gas-phase molecular $O_2$.

## Introduction

Ceria-supported precious and noble metals are attracting much interest due to their unique catalytic properties for demanding reactions related to environmental purifications, fuel-cell applications, and automotive emissions control.[1,2] In the automotive three-way catalyst, the $CeO_2$ support functions as an oxygen buffer by releasing oxygen under reducing conditions and storing oxygen under oxidizing conditions.[3] Thus, the reduction of NOx and the oxidation of CO and hydrocarbons can be accomplished simultaneously under dynamic automotive cyclic fuel-lean and fuel-rich conditions. Supported Pt/$CeO_2$ catalysts have also been found to preferentially oxidize trace amounts of CO in a $H_2$-rich environment, and this is referred to as PROX (preferential oxidation).[4,5] It is widely accepted that the unique properties of the supported metal/$CeO_2$ system stems from the presence of abundant $Ce^{3+}$−$Ce^{4+}$ coupling within the $CeO_2$ structure. The $Ce^{3+}$/$Ce^{4+}$ ratio undergoes dynamic change responding to its environment, such as fuel-lean and -rich conditions, which makes $CeO_2$ an oxygen reservoir for the supported precious metals.

Recently, spectroscopic evidence showing that $CeO_2$ is an active support for precious metals has been achieved. The $CeO_2$ support was found to spontaneously oxidize its supported noble metals. Smirnov and Graham[6] have used XPS spectroscopy to monitor the oxidation state of Pd dispersed on a $CeO_2$−$ZrO_2$ film. The supported Pd was observed to become oxidized by the ceria support in the absence of gas-phase oxygen, thus giving direct spectroscopic evidence for the transfer of oxygen from the $CeO_2$ to its supported noble metal. This result is in parallel with a previous temperature-programmed desorption study, in which oxygen migration from the $CeO_2$ support to the supported Rh metal was evidenced by the observation of a substantial amount of $CO_2$ following heating up the preadsorbed CO on Rh sites that were dispersed on the $CeO_2$ substrate.[7] It is worth noting, however, that the above examples[6,7] were based on model systems in which precious metals were dispersed on the $CeO_2$ or $CeO_2$−$ZrO_2$ films.

In practical applications, $CeO_2$ powder may undergo significant textural changes under reaction conditions. For examples, $CeO_2$ undergoes severe surface area loss under reducing conditions and this also leads to agglomeration of the supported precious metals.[8] Another result of the precious metal−$CeO_2$ interaction was found to be geometric decoration of the precious metal by the $CeO_2$ support, a phenomenon known as SMSI (strong metal−support interaction) that was initially observed in the $TiO_2$-supported noble metal systems.[9] A TEM study has shown that the surface of Pt was progressively covered by the $CeO_2$ support when the catalyst is subjected to $H_2$ treatment at certain temperatures (>500 °C). This geometric decoration consequently leads to severe decrease of the Pt chemisorption capacity.[9−11]

Various characterization techniques have been employed to investigate the metal−support interaction in the precious metal/$CeO_2$ catalytic system, among which transmission electron microscopy (TEM), X-ray photoelectron spectroscopy (XPS), and Fourier transform infrared spectroscopy (FT-IR) are the

* Corresponding author phone: (610) 758-4274; fax: (610) 758-5057; e-mail: iew0@lehigh.edu.

[†] Operando Molecular Spectroscopy and Catalysis Laboratory and Chemical Engineering Department.

[‡] Center for Advanced Materials and Nanocharacterization and Materials Science & Engineering Department.

10.1021/jp710591m CCC: $40.75 
Published on Web 03/26/2008

most popular ones. Recently, Raman spectroscopy has been demonstrated as an effective and easy tool to probe the state of the supported noble metals Pd, Pt, and Rh.[12−18] Special attention was paid to the metal−oxygen vibration signals for their qualitative value in reporting the oxidation state of noble metals, which is a very important factor in revealing the catalytic mechanism. Raman signals of Pt−O, Pd−O, and Rh−O vibrations of ceria-supported precious metal oxides were first reported by Murrell et al.[17] Brogan and Dines[16] performed a systematic Raman study of the supported $Pt/Al_2O_3-CeO_2$ catalyst prepared by the sol−gel method. Distinct Raman signals at 550 and 690 $cm^{-1}$ were assigned to Pt−O−Ce and Pt−O vibrations, respectively. The Pt−O−Ce and Pt−O band could be eliminated by $H_2$ treatments. Studies of the behaviors of these vibrations under different environments revealed the strong interaction between Pt and the $CeO_2$ support. Interestingly, Pt supported on $Al_2O_3$ exhibits a broad Raman band at 600 $cm^{-1}$ under an oxygen environment that is also removed by a reducing environment.[18] While the Raman signals of precious metal oxides have been used to probe oxidation and reduction of the noble metals, prior investigations have not examined the simultaneous redox behavior of the precious metal and the oxide support. This dynamic correlation is obviously highly desirable in order to establish the mutual interactions between the precious metals and their supports.

The objective of this investigation is to establish direct spectroscopic evidence for precious metal−support interactions in the $Pt/CeO_2$ catalytic system by simultaneously combining time-resolved in situ Raman and IR spectroscopic measurements[19] during redox treatments. Thus, both the oxide support and the supported Pt will simultaneously be spectroscopically monitored as a function of reducing and oxidizing conditions as well as a function of time. The size domain of the supported Pt and PtOx nanoparticles (NPs) will be determined by scanning transmission electron spectroscopy (STEM) studies. Comparative studies with supported $Pt/SiO_2$ and $Pt/Al_2O_3$ catalytic materials are also undertaken to compare the behavior of Pt supported on $CeO_2$ with Pt supported on other oxide support materials.

## Experimental Section

**Catalyst Synthesis.** The supported $Pt/SiO_2$, $Pt/Al_2O_3$, and $Pt/CeO_2$ catalysts were prepared by the incipient wetness impregnation method with an aqueous solution of $Pt(NH_2)_4(NO_3)_2$ (Aldrich, Pt ≥ 50%) onto $SiO_2$ (Cabot, Cab-O-Sil EH5, 330 $m^2/g$), $Al_2O_3$ (Engelhard/BASF, H5433C, 178 $m^2/g$), and $CeO_2$ (Rhodia, lot 04004401 AC 5, 200 $m^2/g$). The oxide supports were calcined in air at 500 °C for 3 h prior to impregnation. The freshly impregnated samples were kept under ambient conditions for 24 h followed by calcination at 500 °C in air for 3 h at a ramping rate of 1 °C/min from room temperature to 500 °C.

**In Situ Raman and IR Spectroscopy.** The vibrational spectroscopic measurements were performed with a Horiba-Jobin Yvon LabRam-IR system that combined Raman and FT-IR with a confocal microscope. The Raman laser beam and the IR source beam were concentrically aligned so that both spectra could be collected from the same sample spot (the spot size of IR is typically larger than the spot size of Raman). The LabRam-IR system could also be continuously switched between the Raman and IR collection modes so that parallel time-resolved Raman and IR spectra could be collected.

The Raman spectra were collected with a single-stage monochromator (LabRam-HR) with a focal length of 800 mm and 900 grooves/mm grating (Horiba Jobin Yvon, 53011140HR), and a $LN_2$ cooled CCD detector (Horiba Jobin Yvon-CCD 3000 with 2048 × 13.5 $\mu m^2$ pixels). The Raman excitation was achieved with a 532 nm Nd-YAG laser. A 50× objective (Olympus BX-30) was employed for both focusing the laser beam on the sample and collection of the scattered photons. The Rayleigh scattering component was blocked by a notch filter (Kaiser Super Nothch) having ∼100 $cm^{-1}$ cutoff. The chosen operating conditions (800 mm focal length, 200 $\mu$m confocal hole size, and 900 grooves/mm grating) provided a Raman spectral resolution of ∼2 $cm^{-1}$. Typical Raman spectral collection times were 100 s (20 s/scan and 5 scans/spectrum). The Raman spectra were calibrated by using the Hg 546.07 nm line and the Si 520.07 $cm^{-1}$ shift.

FT-IR measurements were performed with a Sense IR system attached at the top of the Horina-Jobin Yvon LabRam HR system. The FT-IR spectrometer is equipped with a $LN_2$-cooled mercury−cadmium−telluride (MCT) detector that has a spectral resolution of 4 $cm^{-1}$. FT-IR spectra were collected in the diffuse reflectance mode by use of a total-reflecting objective (Gas-segrain/Schwarzschild type). FT-IR spectral collection time was typically 36 s (0.3 s/scan and 120 scans). The absorbance spectrum was calculated as

$$\text{absorbance}_{\text{sample}} = -\log_{10}\left(\frac{\text{reflection}_{\text{sample}}}{\text{reflection}_{\text{KCl}}}\right)$$

The KCl spectrum was measured at 200 °C under flowing Ar in the environmental cell described below.

For the in situ Raman and IR spectroscopic studies, about 20 mg of the catalyst sample in loose powder form was placed at the center of the heating stage of an environmental cell (Linkam THMS 600) with the total gas flow maintained at 30 $cm^3$/min. The environmental cell was equipped with a $CaF_2$ window (International Crystal Laboratories) to allow simultaneous Raman and IR spectroscopic measurements. The oxidizing and reducing environments correspond to 3% $O_2$ and 3% $H_2$ balanced by Ar, respectively. During heating and cooling, the sample temperature was linearly programmed at 15 °C/min with an electronic controller and independently calibrated by use of a separate thermal couple embedded in the catalyst sample. At each temperature, 30 min was typically employed for the catalyst sample to reach equilibration in the different environments. Methanol chemisorption IR was used to probe the surface of the freshly calcined and reduced (300 °C) $Pt/CeO_2$ sample. Thus the freshly calcined samples were first heated at 400 °C for 30 min in flowing $O_2$ or $H_2$ (to reduce the sample) and cooled down to 120 °C in $O_2$ and $H_2$, respectively. The oxidized and reduced samples were then exposed to methanol gas, obtained by bubbling Ar through methanol liquid. The flow rate of Ar was regulated to allow a $CH_3OH$ flow of 4 mmol/min (gas). IR spectra were taken after 20 min of methanol follow and a subsequent 10 min of pure Ar flow. During the combined time-resolved Raman/IR measurements, the total-reflecting objective (Gas-segrain/Schwarzschild type) was employed for both Raman and IR spectroscopic measurements to save time. (It was found the lens embedded in the IR objective can be used for Raman measurement.) For these time-resolved measurements, the Raman and IR spectra were each recorded in 20 s (1 scan for Raman and 66 scans for IR), which corresponds to a time resolution of 40 s per complete Raman/IR cycle.

**Isotopic $^{18}O_2$ Experiments.** During isotopic $^{18}O_2$ experiments with the supported $Pt/CeO_2$ catalyst at 300 °C, special care was taken to remove any residual $^{16}O_2$ that may exist in the dead

volume of the switching valve. Thus, $^{16}O_2$ was first replaced by $^{18}O_2$ (2% balanced by He and Ar mixture at 30 $cm^3$/min) at 300 °C after 20 min treatment by $^{16}O_2$, allowing $^{18}O_2$ to flow for 10 min before the initial reduction by $H_2$ at the same temperature. (The first 10 min of $^{18}O_2$ treatment did not induce the isotopic shift of the Pt−O vibration.) The catalyst was then treated with $H_2$ (3% balanced by Ar) flow. After 30 min of $H_2$ treatment at 300 °C, the feeding gas was switched to $^{18}O_2$ and held for an additional 30 min.

**ScanningTransmission Electron Microscopy Analysis.** Samples of the three catalysts (Pt supported on $SiO_2$, $CeO_2$, and $Al_2O_3$) were prepared for STEM characterization by by suspending them in high-purity ethanol and allowing a drop of the suspension to dry on a lacey carbon film supported by a 300-mesh Cu TEM grid. High-angle annular dark-field (HAADF) imaging was carried out on a JEOL 2200FS FEG-STEM operating at 200 keV and equipped with a CEOS spherical-aberration corrector.[20] Subsequent X-ray energy-dispersive spectroscopy (XEDS) analysis was carried out on a VG HB603 FEG-STEM operating at 300 keV and equipped with a Nion Inc. spherical aberration corrector.[21,22] STEM−XEDS spectrum images were collected on an Oxford Instruments XEDS system with a pixel resolution of 128 × 128 and an acquisition time of 200 ms/pixel. After the data acquisition, multivariate statistical analysis (MSA) of the XEDS data was performed with MSAX-ESP v0.11 (M. Watanabe, 2005). MSA is a set of processing techniques that analyzes the spectrum image data cube as a whole and identifies the various components within it that vary independently, and this allows the operator to significantly reduce the inherent background noise from the processed data.[23,24] Watanabe and co-workers[25] have shown that the application of MSA to STEM−XEDS spectrum imaging can significantly improve the quality and interpretability of the acquired data.

## Results

**STEM−HAADF Imaging and XEDS Analysis.** Representative HAADF images of the three supported Pt catalysts are shown in Figure 1 in their oxidized state. The large atomic-number ($Z$) contrast produced by the HAADF imaging technique clearly reveals the Pt species against the $SiO_2$ and $Al_2O_3$ supports. In the $Al_2O_3$-supported catalyst, the particles ranged in size from 0.5 to 3 nm with the dominant size being 1.5 nm. The size of the $SiO_2$-based catalyst was found to exhibit a bimodal Pt particle size distribution of 1−1.5 and 4−7 nm.

In comparison, it is difficult to discern any discrete Pt particles in the HAADF images from the $CeO_2$-supported catalyst (Figure 1). Interpretation of the images from this catalyst was complicated by the high atomic number of the Ce atoms in the underlying $CeO_2$ support ($Z^{Ce} = 54$). Since the contrast in HAADF images is proportional to $Z^2$, the contribution to the overall image contrast from the $CeO_2$ support is large and, consequently, the supported Pt species ($Z^{Pt} = 78$) do not stand out as strikingly in these images as in those acquired from the lighter $Al_2O_3$ and $SiO_2$ supports (where $Z^{Al} = 13$ and $Z^{Si} = 14$, respectively).

STEM−XEDS spectrum imaging was carried out on the supported $Pt/CeO_2$ sample in order to accurately determine the nature of the Pt dispersion on the $CeO_2$ support. The resulting elemental maps, shown in Figure 2, do not reveal any discrete Pt particles. Instead, the Pt Lα signal originates from an area that is spatially coincident with that of the Ce Lα and O Kα signals. The veracity of these data is confirmed by the summed XEDS spectrum (also Figure 2) extracted from the area of the sample indicated by the dashed line in the ADF image. The Pt Mα, Lα, and Lβ peaks are clearly present in excess of the X-ray continuum background. Thus, these data confirms that the Pt is very highly dispersed over the entire $CeO_2$ surface.

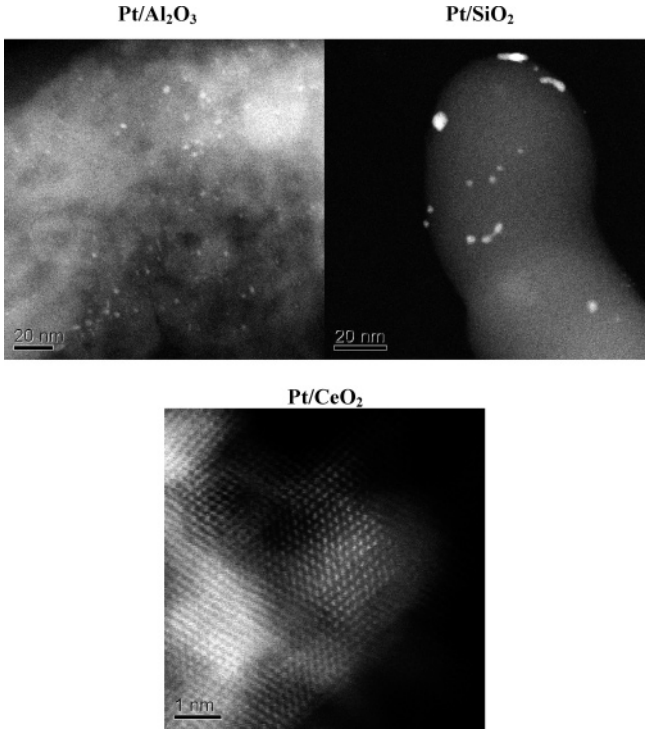


**Figure 1.** STEM-HAADF images of supported $Pt/Al_2O_3$, $Pt/SiO_2$, and $Pt/CeO_2$ catalysts.

**Raman Spectra under Ambient Conditions.** The Raman spectra of the freshly calcined supported $Pt/SiO_2$, $Pt/Al_2O_3$, and $Pt/CeO_2$ catalysts and the crystalline $PtO_2$ reference under ambient conditions are presented in Figure 3. The crystalline $PtO_2$ reference Raman spectrum exhibits two sharp bands at 504 and 545 $cm^{-1}$, which have been assigned to $A_{1g} + E_g$ vibrational modes.[26] According to the literature, amorphous $PtO_2$ gives rise to a band at 610 $cm^{-1}$;[26] crystalline PtO possesses Raman features at 438 ($E_g$) and 657 $cm^{-1}$ ($B_{1g}$);[26] and metallic Pt is not Raman-active. Other bulk platinum oxide phases formed under high-temperature and high-pressure conditions also display distinct Raman features in the <800 $cm^{-1}$ region.[26]

For the supported $Pt/Al_2O_3$ catalyst, only a broad Raman band centered at 610 $cm^{-1}$ is present from PtOx since the $\gamma$-alumina support used in this study does not give rise to Raman-active vibrations.[27] The 610 $cm^{-1}$ vibration is consistent with the vibration of amorphous $PtO_2$ nanoparticles (∼1.5 nm) as suggested by the TEM image in Figure 1. The Raman spectrum of the supported $Pt/SiO_2$ catalyst displays bands at 450, 504, 545, 610, 790, and 1100 $cm^{-1}$. The bands at 450, 790, and 1100 $cm^{-1}$ are vibrations from the $SiO_2$ support[28] and are not affected by $H_2$ reduction (see in situ Raman results below). The sharp vibrations at 504 and 545 $cm^{-1}$ correspond to crystalline $PtO_2$ particles,[26] which are easily reduced by $H_2$ (see results below). The broad signal at 610 $cm^{-1}$ contains contributions from the $SiO_2$ support and amorphous $PtO_2$ vibrations. The amorphous $PtO_2$ band can be easily reduced with $H_2$ (see in situ Raman results below). The presence of two types of supported $PtO_2$ NPs on $SiO_2$, crystalline, and amorphous $PtO_2$ phases is in good agreement with the TEM results, which show dual particle size distribution. The amorphous $PtO_2$ NPs on $SiO_2$ (Raman band at 610 $cm^{-1}$) are probably ∼1.0−1.5 nm, as imaged in Figure

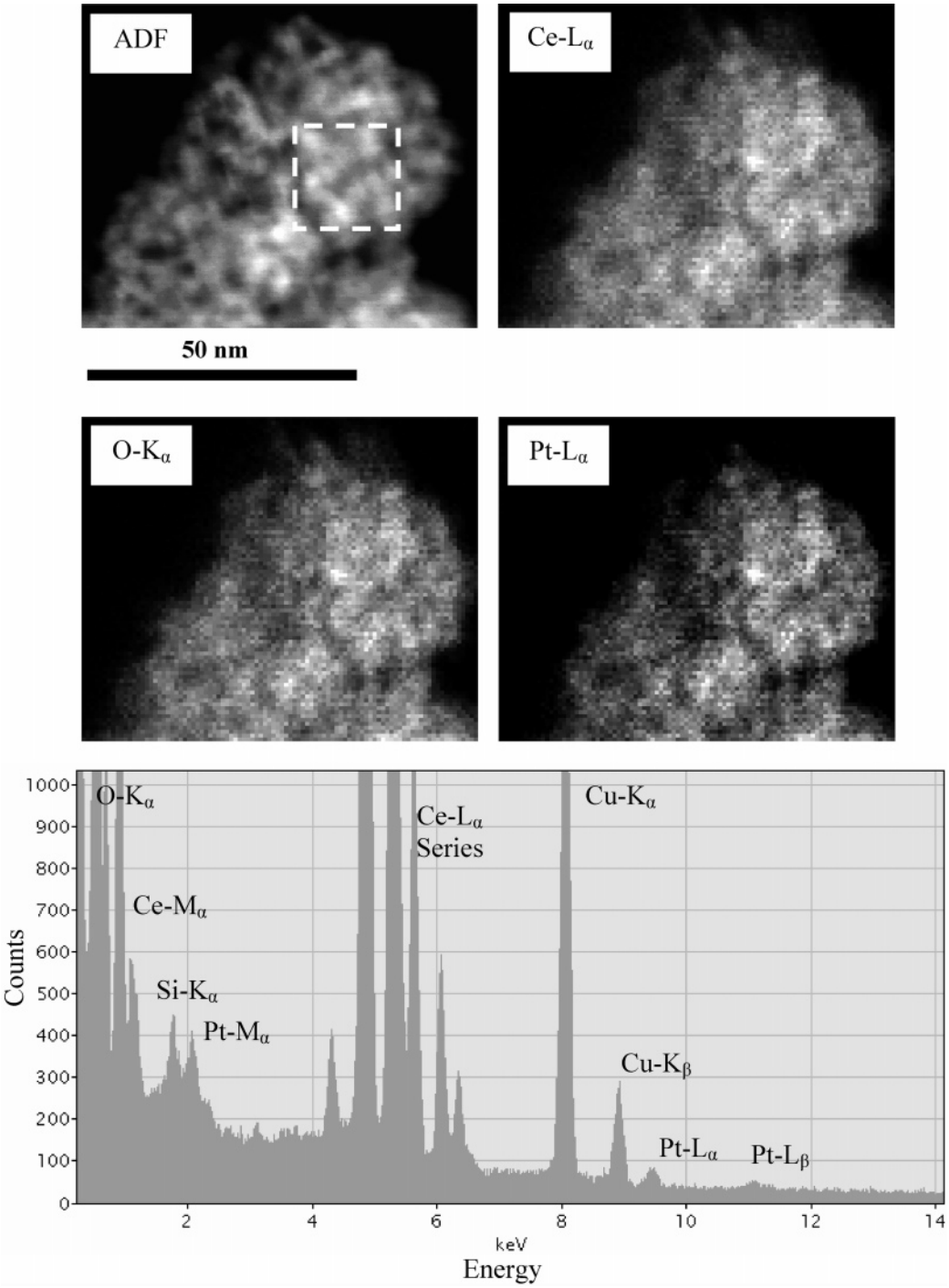


**Figure 2.** STEM-ADF image of the supported Pt/$CeO_2$ catalyst and the corresponding Ce Lα, O Kα, and Pt Lα XEDS maps after background subtraction, showing no discrete Pt particles in this sample. The XEDS spectrum extracted from the area of the sample indicated by the dashed box in the ADF image is also presented. The presence of Pt is clearly indicated by the Pt Lα and L$\beta$ peaks. The Si Kα and Cu Kα,$\beta$ peaks are also visible in the spectrum; these arise from internal fluorescence of the Si(Li) XEDS detector and the Cu TEM grid, respectively.

1, and the crystalline $PtO_2$ particles (Raman band 504 and 545 $cm^{-1}$) are probably 4−7 nm in size, as imaged in Figure 1.

The calcined supported Pt/$CeO_2$ catalyst sample exhibits Raman bands at 450, 550, and 665 $cm^{-1}$. The strong 450 $cm^{-1}$ vibration is associated with the $F2\,g$ symmetry of the crystalline $CeO_2$ support.[29] The Raman features at 550 and 665 $cm^{-1}$ are from the supported PtOx phase and disappear upon reduction and reappear upon oxidation (see in situ Raman studies below). These Raman bands are associated with a highly dispersed surface PtOx phase on $CeO_2$[17] and are tentatively assigned to the bridging Pt−O−Ce vibration (550 $cm^{-1}$) and Pt−O vibration (665 $cm^{-1}$).[16] The band at 400 $cm^{-1}$ is assigned to defect sites[30] on $CeO_2$ induced by coordination of the PtOx to the ceria support. The above findings demonstrate that the state of supported PtOx phase after calcination strongly depends on the specific oxide support.

**In Situ Raman and IR Spectra Acquired under $H_2$ Reducing Conditions.** The Raman spectra of the supported Pt catalysts and bulk $PtO_2$ at elevated temperatures and under $H_2$ reducing conditions are presented in Figure 4. Prior to exposure to the reducing $H_2$/Ar environment, the bulk $PtO_2$ and supported PtOx catalysts were initially calcined in flowing $O_2$/Ar at 350 °C and subsequently cooled down to 50 °C. Bulk $PtO_2$ was readily reduced to metallic Pt at 50 °C by exposure to the

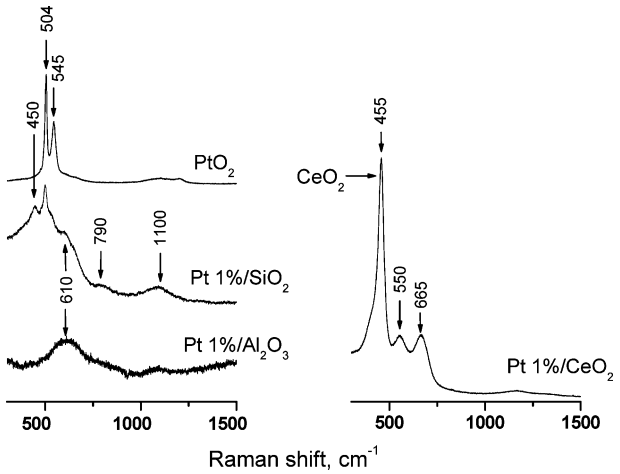


**Figure 3.** Raman spectra of supported $Pt/SiO_2$, $Pt/Al_2O_3$, and $Pt/CeO_2$ measured under ambient conditions. A spectrum of crystalline $\alpha$-$PtO_2$ is shown for comparison. Insets display corresponding XPS spectra of supported $Pt/CeO_2$.

reducing environment as shown in Figure 4a. The in situ Raman spectra of the supported PtOx catalysts at 50 °C reveal that the supported PtOx phases are oxidized and unchanged from those present under ambient conditions (see Figure 3). Switching from the oxidizing to the reducing environment at 50 °C results in reduction of the supported amorphous $PtO_2$ phases present in the supported $Pt/Al_2O_3$ catalyst and the amorphous and crystalline $PtO_2$ phase present in the supported $Pt/SiO_2$ catalyst systems (see Figure 4b,c). The remaining Raman features at 450, 486, and 610 $cm^{-1}$ in the supported $Pt/SiO_2$ spectrum are from the $SiO_2$ support.[29] In contrast to these systems containing bulk $PtO_2$ phases, the supported PtOx phase on $CeO_2$ is much more difficult to reduce with $H_2$ and reduction initiates at 200 °C as shown in Figure 5a. Clearly, the PtOx−$CeO_2$ interaction is very different than the PtOx−$SiO_2$ and PtOx−$Al_2O_3$ interactions.

The corresponding in situ IR spectra are focused on the surface OH stretching region of the supported PtOx catalysts. For the supported $Pt/SiO_2$ and $Pt/Al_2O_3$ catalysts, the IR bands in the surface OH region are not perturbed by the reduction treatment since both of these oxide supports are not reducible (spectra not shown). The IR bands in the surface OH region for the supported $Pt/CeO_2$ catalysts, however, do undergo changes during reduction as indicated in Figure 5b. The IR bands of $CeO_2$ at 3695 and 3655 $cm^{-1}$ are assigned to type I and II hydroxyl groups, designated as OH(I) and OH(II), respectively. The OH(I) vibration originates from isolated surface hydroxyl groups on the $CeO_2$ surface, and the OH (II) band has been assigned to bridging surface hydroxyl groups.[31] Both type I and II surface hydroxyls are present in the 50−200 °C temperature range under reducing conditions for the supported $Pt/CeO_2$ catalyst. At 300 °C, however, the IR band associated with the isolated surface OH(I), at 3695 $cm^{-1}$, is not present due to its removal while the surface OH(II) band shifts to lower wavenumber. Exposure of the Pt-free $CeO_2$ support to the same reducing conditions, however, does not cause reduction of the surface hydroxyls (see Figure 5c). This suggests that depletion of surface OH(I) hydroxyls is induced by $H_2$ spillover from the metallic Pt. Thus, the IR signals of the surface hydroxyls can be thought of as in situ probes for the oxidation state of the $CeO_2$ support. The present findings for the reduction of supported $Pt/CeO_2$, $Pt/SiO_2$, $Pt/Al_2O_3$, and $CeO_2$ are in excellent agreement with earlier $H_2$-TPR studies reported in the literature.[32−36]

The above conclusions were also chemically probed via in situ $CH_3OH$ chemisorption IR studies because the C−O

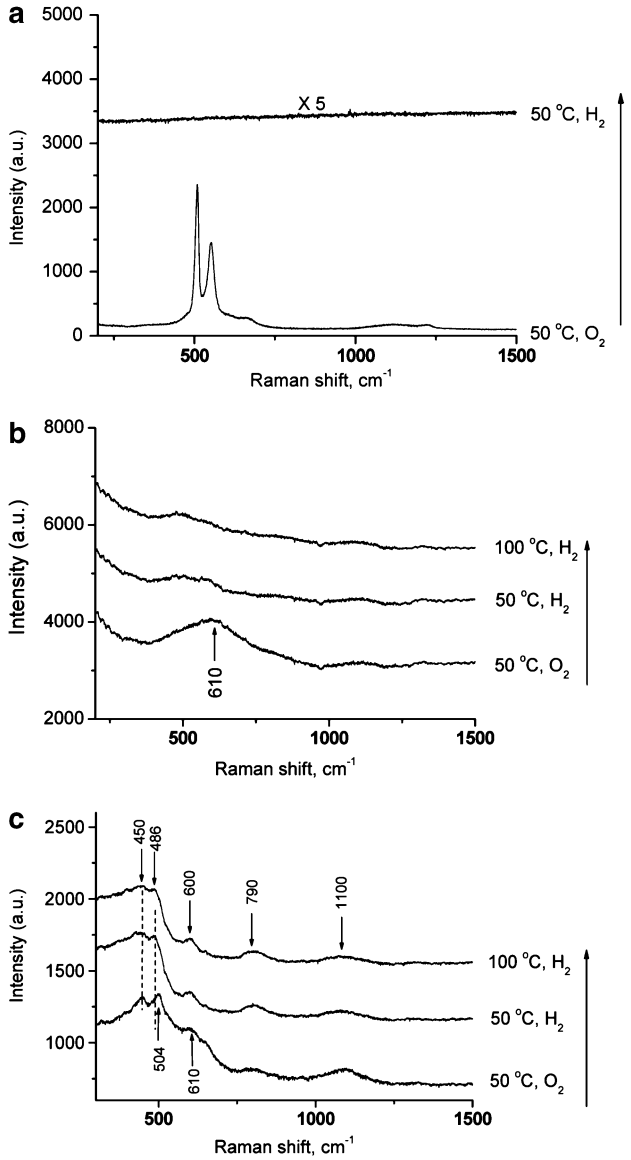


**Figure 4.** In situ Raman spectra of (a) $\alpha$-$PtO_2$, (b) supported $Pt/Al_2O_3$, and (c) supported $Pt/SiO_2$ samples under $H_2$/Ar flow (3% balanced by Ar, total flow 30 $cm^3$/min) at elevated temperatures. The catalysts were first heated in $O_2$/Ar flow at 350 °C for 30 min followed by cooling down to 50 °C in $O_2$/Ar flow and subsequent exposure to $H_2$/Ar flow at elevated temperatures.

vibration of the surface methoxy group, $CH_3O^*$, is known to be sensitive to the surface oxidation state of $CeO_2$.[31] The $CH_3$-OH IR spectra of freshly calcined and reduced $Pt/CeO_2$ following exposure of $CH_3OH$/He at 150 °C are shown in Figure 5d. The IR bands at 1091 and 1036 $cm^{-1}$ have been assigned to the surface methoxy C−O stretching vibrations at sites I and II, respectively.[31] The IR spectrum of the calcined PtOx/$CeO_2$ sample displays the C−O vibrations of both the surface methoxy(I) and (II) groups, but only the surface methoxy(II) C−O IR vibration is present in the spectrum after $H_2$ reduction. The $CH_3OH$ IR measurements of the supported $Pt/CeO_2$ catalysts further confirm that the surface OH(I) sites are removed upon $H_2$ reduction at elevated temperatures.

**In Situ Raman and IR Spectroscopy during Reoxidation and Rereduction.** Reoxidation of the reduced bulk Pt metallic powder at elevated temperatures does not re-form crystalline $PtO_2$ because the bulk $PtO_2$ phase is thermally unstable at elevated temperature and decomposes to metallic Pt.[37] Reoxidation of the supported $Pt/SiO_2$ catalyst after reduction at

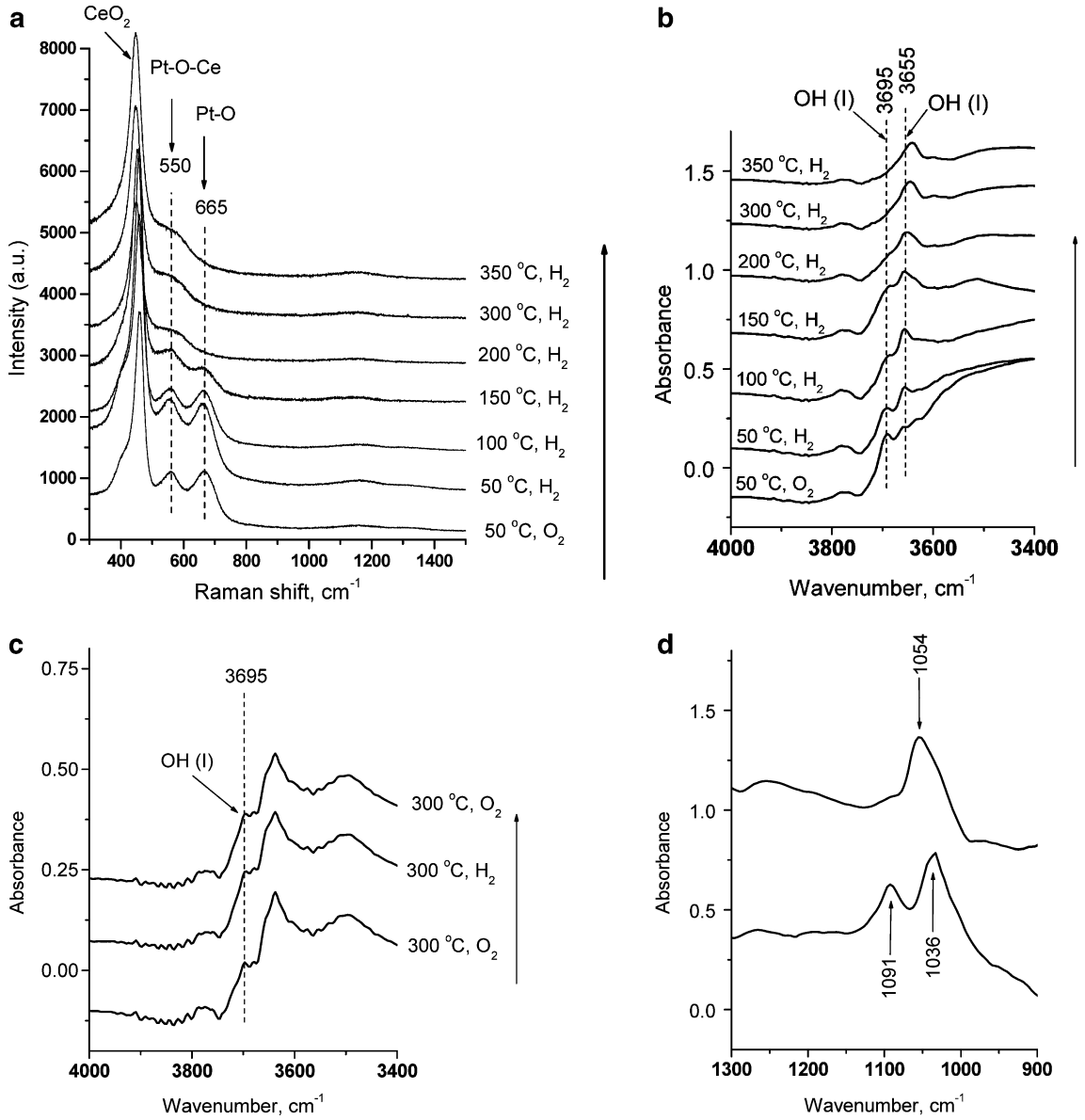


**Figure 5.** Combined in situ (a) Raman and (b) IR spectra of supported $Pt/CeO_2$ catalyst under $H_2/Ar$ flow (3% balanced by Ar, total flow 30 $cm^3$/min) at elevated temperatures. In situ IR spectra of (c) $CeO_2$ support under flowing cyclic $O_2-H_2$ treatments at 300 °C and (d) supported $Pt/CeO_2$ adsorbing $CH_3OH$ at 120 °C are shown as references.

200 °C does not regenerate the initial crystalline $PtO_2$ NPs (not shown). Reoxidation of the supported $Pt/Al_2O_3$ catalyst after reduction at 200 °C gives rise to only a trace of amorphous $PtO_2$ NPs (not shown). The corresponding in situ IR spectra do not indicate any detectable changes in the surface OH region of the $Al_2O_3$ and $SiO_2$ supports (not shown).

In contrast, reoxidation of the 200 °C reduced supported $Pt/CeO_2$ catalyst results in almost complete regeneration of the supported PtOx phase on $CeO_2$ as shown in Figure 6. Reoxidation of the 300 °C reduced supported $Pt/CeO_2$ catalyst, however, does not result in complete regeneration of the supported PtOx phase as shown in Figure 7a. The corresponding IR spectra of the surface OH region, as shown in Figure 7b, reveal that the surface OH(I) vibration at 3695 $cm^{-1}$ is absent under reducing conditions and present under oxidizing conditions. Thus, the metal−support interaction of the supported $Pt/CeO_2$ catalyst system gives rise to reversible reduction−oxidation cycles at modest temperatures (200 °C) but incomplete redispersion at the higher temperature of 300 °C.

The degree of oxidative regeneration of the supported $Pt/CeO_2$ catalyst system was further probed by a second reduction treatment in $H_2/Ar$. The 200 °C reduced and reoxidized supported $Pt/CeO_2$ catalyst was found to exactly reproduce the initial reduction behavior shown in Figure 5a,b, which indicates the complete reversibility of the reduction−oxidation processes at 200 °C. The 300 °C reduced and reoxidized supported $Pt/CeO_2$ catalyst, however, was found to readily reduce at 50 °C as indicated by in situ Raman spectroscopy (see Figure 8) and the surface OH(I) sites were almost completely reduced at 150 °C (not shown). Consequently, the presence of a small fraction of metallic Pt NPs, due to incomplete redispersion at 300 °C, is sufficient to cause hydrogen spillover and accelerate the reduction of the dispersed PtOx phase and the $CeO_2$ support at much milder temperatures.

Furthermore, surface peroxo, $O_2^{2-}$ (825 $cm^{-1}$), and superoxo, $O_2^-$ (1125 $cm^{-1}$), species are not present in the in situ Raman and IR spectra during the present reduction−reoxidation treatments.[30]

**Time-Resolved in Situ Raman and IR Spectroscopic Study of Reduction and Reoxidation of Supported $Pt/CeO_2$.** Time-resolved in situ Raman and IR spectroscopic measurements, at 20 s intervals for each, were also undertaken to obtain additional

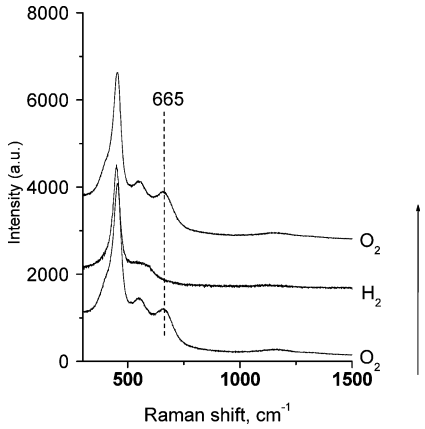


**Figure 6.** In situ Raman spectroscopic monitoring of reduction and subsequent reoxidation of supported $Pt/CeO_2$ catalyst at 200 °C. The catalyst was first reduced by exposure to flowing $H_2$/Ar at 200 °C for 30 min. Reoxidation of the catalyst was carried out by switching to flowing $O_2$/Ar at the same temperature for 30 min.

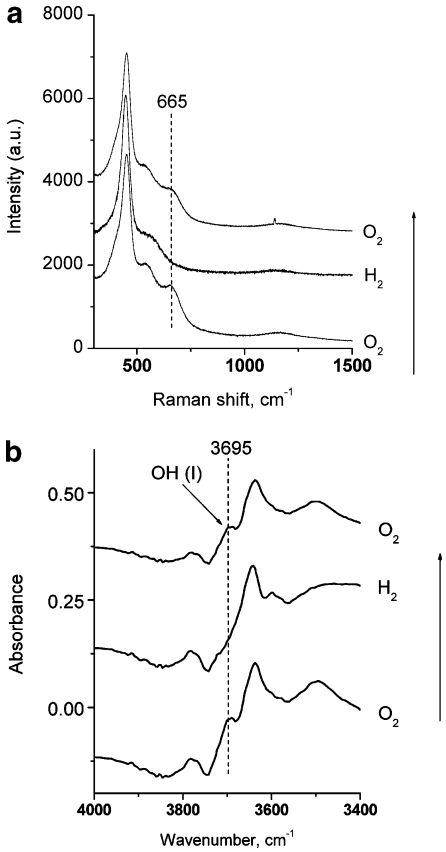


**Figure 7.** In situ (a) Raman and (b) IR spectroscopic monitoring of reduction and reoxidation of supported $Pt/CeO_2$ catalyst at 300 °C. The catalyst was first reduced by exposure to flowing $H_2$/Ar at 300 °C for 30 min. Reoxidation of the catalyst was carried out by switching to flowing $O_2$/Ar at the same temperature for 30 min.

insights into the reduction and reoxidation processes of the supported $Pt/CeO_2$ catalyst at 300 °C. The PtOx vibration at 665 $cm^{-1}$ was monitored with Raman and the $CeO_2$ surface OH(I) vibration at 3695 $cm^{-1}$ was monitored with IR at 300 °C. The normalized intensities of the PtOx and surface OH-(I) vibrations are plotted as a function of time during reduction and reoxidation in Figure 9 panels a and b, respectively. During the initial reduction in $H_2$/Ar, the PtOx vibration decreases slightly faster than the $CeO_2$ surface OH(I) vibration. This trend suggests that the reduction of the supported PtOx phase precedes that of the $CeO_2$ support and is most likely related to $H_2$ spillover

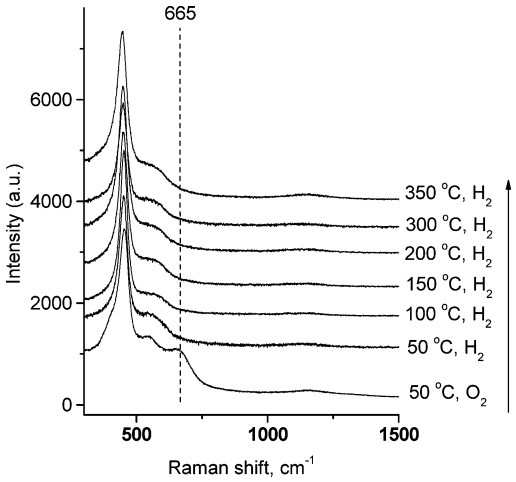


**Figure 8.** In situ Raman spectroscopic monitoring of the secondary reduction of the supported $Pt/CeO_2$ catalyst. The catalyst was first reduced and reoxidized at 300 °C (refer to Figure 7 for detail) and cooled down to 50 °C in $O_2$/Ar. The secondary reduction was carried out by switching to $H_2$/Ar flow at elevated temperatures with 30 min duration at each temperature.

from the reduced Pt sites. Reoxidation of the reduced catalyst reveals that the $CeO_2$ surface OH(I) vibration is restored before reoxidation of the supported metallic Pt phase. This trend suggests that oxidation of the ceria support precedes oxidation of the supported metallic Pt phase and that Pt redispersion may require the presence of $CeO_2$ surface OH(I) sites. In summary, the time-resolved reduction−reoxidation cycles reveal the complex dynamic interplay between the supported Pt phase and the $CeO_2$ support in different reactive environments.

**In Situ Raman and IR Spectroscopic Measurements during Reoxidation with Isotopic Molecular $^{18}O_2$.** Additional insights into the reoxidation process were obtained by employing $^{18}O_2$ as the oxidizing agent for the reduced supported $Pt/CeO_2$ catalyst. Raman spectra of the freshly calcined supported $Pt/CeO_2$ catalyst are shown under consecutive $^{16}O_2$/Ar, $H_2$/Ar, and $^{18}O_2$/Ar environments at 200 °C in Figure 10. The behavior of the supported PtOx Raman band at 665 $cm^{-1}$ follows the behavior already seen for reduction and reoxidation in Figure 6. However, employing $^{18}O_2$ to reoxidize the reduced supported Pt phase did not lead to $Pt^{18}Ox$ formation since $Pt^{18}Ox$ is expected to vibrate ∼20−30 $cm^{-1}$ lower than $Pt^{16}Ox$.[38] The parallel in situ IR data (not shown), also indicate restoration of the $CeO_2$ surface $^{16}OH(I)$ sites rather than surface $^{18}OH(I)$ sites. These isotopic oxygen experiments demonstrate that reoxidation of the reduced supported Pt phase and the surface OH(I) sites on $CeO_2$ proceeds with $^{16}O$ from the $CeO_2$ support lattice and not from gas-phase molecular $^{18}O_2$. The role of gas-phase molecular $O_2$ is only to reoxidize the oxygen vacancies in the $CeO_2$ support (i.e., a Mars−van Krevelen mechanism).

The oxygen transfer characteristics of the supported $Pt/CeO_2$ catalyst were further investigated in a $H_2$-rich environment, $H_2/O_2$ ∼50, with isotopically labeled $^{18}O_2$. Under such net reducing conditions at 200 °C, the PtOx phase on $CeO_2$ is completely reduced as shown by the absence of the PtOx Raman band at 665 $cm^{-1}$ in Figure 11. Upon cooling down to 50 °C in the same net reducing gas mixture, the $Pt^{16}Ox$ Raman band at 665 $cm^{-1}$ reappears without the presence of $Pt^{18}Ox$. In the absence of a trace of gas-phase molecular $^{18}O_2$, however, the PtOx Raman band does not regenerate in the flowing $H_2$/Ar environment at 50 °C. The PtOx Raman band at 665 $cm^{-1}$ also does not regenerate at 50 °C in the $H_2/O_2$ environment if the

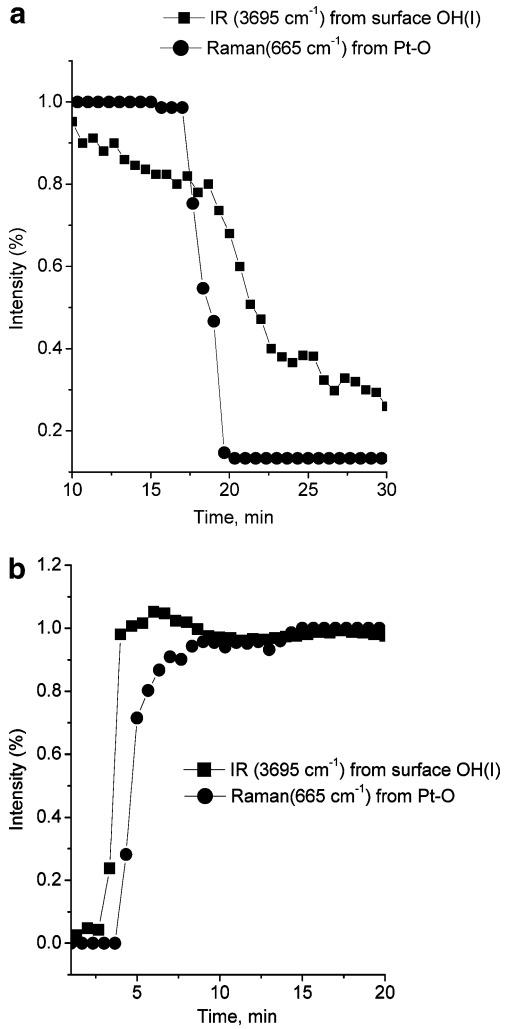


**Figure 9.** Temporal profile of (a) reduction and (b) reoxidation of supported $Pt/CeO_2$ at 300 °C as studied by combined time-resolved Raman and IR spectroscopy. The relative intensities of the surface OH-(I) IR signal of $CeO_2$ at 3695 $cm^{-1}$ and the supported PtOx Raman signal at 665 $cm^{-1}$ are plotted as function of time.

supported $Pt/CeO_2$ catalyst was previously reduced at 300 °C, where some metallic Pt NPs are also present on $CeO_2$.

## Discussion

**PtOx Interaction with Oxide Supports under Oxidizing Conditions.** The STEM-ADF images and Raman spectra clearly reflect the interactions of the supported PtOx phase with the underlying oxide supports. The STEM images reveal that the dimension of supported PtOx NPs is as follows: $SiO_2$ (bimodal distribution of ∼1−1.5 and 4−7 nm) > $Al_2O_3$ (∼1.5 nm) > $CeO_2$ (<0.7 nm). The corresponding Raman spectra provide additional structural insights about the supported PtOx phases with crystalline α-$PtO_2$ and amorphous PtOx NPs on $SiO_2$, amorphous PtOx NPs on $Al_2O_3$, and surface PtOx species on $CeO_2$. For the supported $PtOx/SiO_2$ catalyst, the 1−1.5 nm amorphous PtOx NPs correspond to the Raman band at 610 $cm^{-1}$, and the 4−7 nm α-$PtO_2$ NPs give rise to the 504 $cm^{-1}$ Raman band. Thus, the state of the supported PtOx phase is related to the PtOx−support interaction. The Pt densities (grams per square meter) are apparently different on the three supports because of their surface area difference. The fact that $SiO_2$ support has the relatively largest surface area but contains the largest Pt aggregation further confirms its weak interaction with Pt.

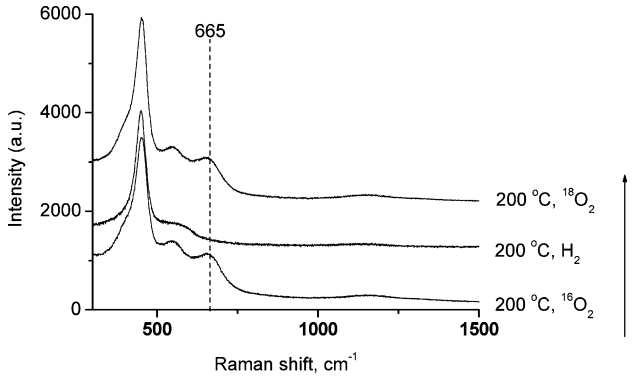


**Figure 10.** In situ Raman spectra of supported $Pt/CeO_2$ under sequential $^{16}O_2$/Ar, $H_2$/Ar, and $^{18}O$/Ar environments at 200 °C.

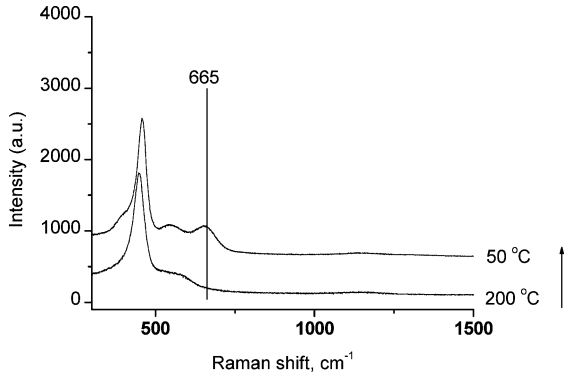


**Figure 11.** In situ Raman spectroscopy during cooling-down of reduced supported $Pt/CeO_2$ catalyst in net reducing environments ($H_2/^{18}O_2$ = 50 with a flow of 100 $cm^3$/min in total). The catalyst was alternatively maintained for 10 min at 50 and 200 °C each with ramping and cooling rates of 10 °C/min.

**PtOx Interaction with Oxide Supports under Reducing Conditions.** The nature of the supported PtOx phase under oxidizing conditions also determines its ease of reduction. The agglomerated amorphous PtOx and α-$PtO_2$ NPs, as well as bulk α-$PtO_2$, readily reduce to metallic Pt at 50 °C in a flowing $H_2$/Ar stream. The highly dispersed surface PtOx species on $CeO_2$, however, require much higher reduction temperature for reduction to metallic Pt. Thus, the stronger interaction of PtOx with the $CeO_2$ support retards reduction of the supported PtOx phase.

In addition, H-spillover from the metallic Pt NPs also reduces the $CeO_2$ surface by reducing the surface OH(I) sites. Direct spectroscopic observation of this H-spillover phenomenon is provided by the time-resolved in situ Raman/IR spectroscopic measurements, which show that the supported PtOx begins reduction to metallic Pt prior to reduction of the $CeO_2$ surface OH(I) sites. Furthermore, the reduction of $CeO_2$ in the absence of Pt normally requires much higher temperatures, closer to 500 °C.

$H_2$-TPR studies have been previously used to elucidate the PtOx−support interaction in the supported $PtOx/CeO_2$ catalytic system.[32−34] The retarded reduction threshold of the surface PtOx species on $CeO_2$ in comparison with the agglomerated PtOx NPs on $Al_2O_3$ and $SiO_2$ has been ascribed to strong electronic interactions between PtOx and the $CeO_2$ support, with the latter tending to keep the former in the oxidized state and preventing it from agglomerating.[39] The present findings also demonstrate that direct Pt−O−Ce bonding is related to the retarded reduction characteristics.

Further increasing the reduction temperature leads to severe textural changes of the $CeO_2$ support that causes a significant loss of its surface area and the agglomeration of metallic Pt as

a consequence.[8] This complex scenario is not the subject of this paper. The present study is dedicated to addressing the fundamental aspects of the PtOx−$CeO_2$ interactions under relatively mild conditions when $CeO_2$ does not undergo sintering.

**PtOx−Support Interactions during Reoxidation of Metallic Pt.** Reoxidation of reduced Pt NPs supported on the $Al_2O_3$ and $SiO_2$ supports does not lead to formation of supported PtOx NPs because the bulk $PtO_2$ phase is not thermally stable at elevated temperatures.[26] Reoxidation of the reduced Pt NPs supported on the $CeO_2$ support, however, results in redispersion of the metallic Pt NPs as surface PtOx species on $CeO_2$. The absence of significant residual metallic Pt NPs suggests that the supported platinum on $CeO_2$ probably consists of much smaller Pt particles than on $Al_2O_3$ and $SiO_2$ supports. It has been proposed that there is a strong affinity between the reduced noble metals and oxygen-deficient sites on the surface of metal oxides.[40] On the $CeO_2$ surface, elimination of surface OH(I) groups may create the oxygen-deficient sites that help to "immobilize" the metallic Pt during reduction. Such a highly dispersed metallic Pt should be easily reoxidized by subsequent oxidation treatments. In the case of the reduced supported Pt/$Al_2O_3$ and Pt/$SiO_2$ catalyst systems, however, oxygen-deficient sites on the $Al_2O_3$ and $SiO_2$ supports are not formed under reducing conditions.

The in situ Raman study also showed that the reoxidation behavior of metallic Pt supported on $CeO_2$ is dependent on the reduction temperature since higher reduction temperatures tend to result in incomplete reoxidation of the supported Pt phase (see Figure 7). This may be related to the dynamic nature of the $CeO_2$ surface that undergoes severe textural changes during reduction at high temperatures.[8] Slight local structural rearrangement of $CeO_2$ at 300 °C may result in the loss of a small fraction of the Pt stabilization sites, which would cause agglomeration of Pt into larger NPs. The aggregated metallic Pt NPs on $CeO_2$ would minimize the Pt−$CeO_2$ interaction and significantly lower the reduction threshold of the supported PtOx during the secondary reduction treatment through H-spillover (see Figure 8 and previous discussion). Thus, the presence of some aggregated metallic Pt NPs on $CeO_2$ facilitates the reduction of the coexisting supported PtOx phase on $CeO_2$.

**Source of Oxygen for Reoxidation of Metallic Pt.** The oxygen transfer process represents a unique aspect of $CeO_2$-supported metal catalysts. The isotopic molecular $^{18}O_2$ exchange studies (see Figures 10 and 11) clearly demonstrate that metallic Pt is reoxdized to PtOx with lattice oxygen from the $CeO_2$ support, even at relatively low temperatures. Consequently, the gas-phase molecular $O_2$ functions only to reoxidize the $CeO_2$ bulk lattice (Mars−van Krevelen mechanism). The oxidation of metallic Pt by the $CeO_2$ support rather than gas-phase molecular $O_2$ is in agreement with the well-known fact that $CeO_2$ possesses large amounts of structurally stable $Ce^{4+}$−$Ce^{3+}$ couples and that the $Ce^{4+}/Ce^{3+}$ ratio undergoes dynamic changes in response to different composition environments. In the supported Pt/$CeO_2$ system, the reduced Pt acts as an oxygen atom acceptor, which decreases the $Ce^{4+}/Ce^{3+}$ ratio of the $CeO_2$ support. In parallel, gaseous molecular $O_2$ gas reacts with reduced $Ce^{3+}$ sites to increase the $Ce^{4+}/Ce^{3+}$ ratio. This result is also consistent with a literature report on oxygen storage dynamics over supported Pt/$CeO_2$ catalysts in that $O_2$ molecule activation does not directly involve Pt but rather the $CeO_2$ surface.[41] The isotopic experiments also suggest a very rapid $^{18}O$ diffusion process from the reduced $CeO_2$ surface into the bulk lattice since the $CeO_2$ surface sites are overwhelmingly populated by surface $^{16}O$ atoms.

## Conclusions

The combination of time-resolved in situ Raman/IR spectroscopy and complementary STEM−XEDS−HAADF microscopic studies is a powerful approach for the study of metal−support interactions. For supported PtOx catalysts, the Raman vibrations can discriminate between crystalline $PtO_2$ (504 $cm^{-1}$) and amorphous $PtO_2$ (610 $cm^{-1}$) NPs as well as surface PtOx species (665 $cm^{-1}$), and STEM−XEDS provides information about the NP size distribution. As the Pt−support interaction increases, the supported PtOx phase goes from crystalline $PtO_2$ to amorphous $PtO_2$ to surface PtOx species. The extent of the Pt−support interaction also determines the ease of reduction of the supported PtOx phase ($SiO_2 \sim Al_2O_3 \gg CeO_2$). Redispersion of the metallic supported Pt NPs to the supported PtOx phase also depends on the extent of the Pt−support interaction ($CeO_2 > Al_2O_3 \sim SiO_2$). For the strongly interacting PtOx/$CeO_2$ system, the supported metallic Pt NPs can be completely redispersed as surface PtOx species if the reduction is conducted under mild temperatures (∼200 °C). For the weakly interacting Pt−$Al_2O_3$ and Pt−$SiO_2$ systems, redispersion of the Pt NPs was not achievable under the oxidation conditions investigated. Reduction of Pt also leads to reduction of reducible supports such as $CeO_2$ due to H-spillover. Reoxidation of metallic Pt NPs on $CeO_2$ was found to occur via bulk lattice oxygen extracted from the $CeO_2$ support rather than gas-phase molecular $^{18}O_2$, even under mild temperatures.

**Acknowledgment.** C.J.K. and A.A.H. gratefully acknowledge funding from the NSF Materials Research Science and Engineering Center (NSF-DMR-0079996).

## References and Notes

(1) Trovarelli, A.; de Leitenburg, C.; Boaro, M.; Dolcetti, G. *Catal. Today* **1999**, *50*, 353.
(2) Kaspar, J.; Fornasiero, P.; Graziani, M. *Catal. Today* **1999**, *50*, 285.
(3) Yao, H. C.; Yao, Y. F. Y. *J. Catal.* **1984**, *86*, 254.
(4) Pozdnyakova, O.; Teschner, D.; Wootsch, A.; Kröhnert, J.; Steinhauer, B.; Bauer, H.; Toth, L.; Jentoft, F. C.; Knop-Gericke, A.; Paál, Z.; Schlögl, R. *J. Catal.* **2006**, *237*, 1.
(5) Wootsch, A.; Descorme, C.; Duprez, D. *J. Catal.* **2004**, *225*, 259.
(6) Smirnov, M. Y.; Graham, G. W. *Catal. Lett.* **2001**, *72*, 39.
(7) Gorte R. J., Zafiris G. S. *J. Catal.* **1993**, *139*, 561.
(8) Perrichon, V.; Laachir, A.; Abouarnadasse, S.; Touret, O.; Blanchard, G. *Appl. Catal., A* **1995**, *129*, 69.
(9) Tauster, S. J.; Fung, S. C.; Garten, R. L. *J. Am. Chem. Soc.* **1978**, *100*, 170.
(10) Bernal, S.; Calvino, J. J.; Cauqui, M. A.; Gatica, J. M.; López Cartes, C.; Pérez Omil, J. A.; Pintado, J. M. *Catal. Today* **2003**, *77*, 385.
(11) Bernal, S.; Calvino, J. J.; Cauqui, M. A.; Gatica, J. M.; Larese, C.; Pérez Omil, J. A.; Pintado, J. M. *Catal. Today* **1999**, *50*, 175.
(12) Borodko, Y.; Ager, J. W., III; Marti, G. E.; Song, H.; Niesz, K.; Somorjai, G. A. *J. Phys. Chem. B* **2005**, *109*, 17386.
(13) Cornaglia, L. M.; Múnera, J.; Irusta, S.; Lombardo, E. A. *Appl. Catal., A* **2004**, *263*, 91.
(14) Graham, G. W.; O' Neill, A. E.; Chen, A. E. *Appl. Catal., A* **2003**, *252*, 437.
(15) Uy, D.; Wiegand, K. A.; O' Neill, A. E.; Dearth, M. A.; Weber, W. H. *J. Phys. Chem. B* **2002**, *106*, 387.
(16) Brogan, M. S.; Dines, T. J. *J. Chem. Soc., Faraday Trans.* **1994**, *90*, 1461.
(17) Murrell, L. L.; Tauster, S. J.; Anderson, D. R. *Catal. Automot. Pollut. Control 2, Proc. Int. Symp., 2nd, 1991* [see *Stud. Surf. Sci. Catal.* **1991**, *71*], 275.
(18) Uy, D.; O'Neill, A. E.; Li, J.; Watkins, W. L. H. *Catal. Lett.* **2004**, *95*, 191.
(19) Bourdon, G. L.; Adar, F.; Moreau, M.; Morel, S.; Reffner, J.; Mamede, A.-S.; Dujardin, C.; Payen, E. *Phys. Chem. Chem. Phys.* **2003**, *5*, 4441.

(20) Watanabe, M.; Ackland, D. W.; Kiely, C. J.; Williams, D. B.; Kanno, M.; Hynes, R.; Sawada, H. *JEOL News* **2006**, *41*, 2.

(21) Lyman, C. E.; Goldstein, J. I.; Williams, D. B.; Ackland, D. W.; Von Harrach, S.; Nichols, A. W.; Statham, P. J. *J. Microsc.* **1994**, *176*, 85.

(22) Watanabe, M.; Ackland, D. W.; Burrows, A.; Kiely, C. J.; Williams, D. B.; Krivanek, O. L.; Dellby, N.; Murfitt, M. F.; Szilagyi, Z. *Microsc. Microanal.* **2006**, *12*, 515.

(23) Trebbia, P.; Bonnet, N. *Ultramicroscopy* **1990**, *34*, 165.

(24) Trebbia, P.; Mory, C. *Ultramicroscopy* **1990**, *34*, 179.

(25) Burke, M. G.; Watanabe, M.; Williams, D. B.; Hyde, J. M. *J. Mater. Sci.* **2006**, *41*, 4512.

(26) McBride, J. R.; Graham, G. W.; Peters, C. R.; Weber, W. H. J. *Appl. Phys.* **1991**, *69*, 1596.

(27) Chan, S. S.; Wachs, I. E.; Murrell, L. L.; Dispenziere, N. C. *J. Catal.* **1985**, *92*, 1.

(28) Sharma, S. K.; Cooney, T. F.; Wang, Z.; van der Laan, S. *J. Raman Spectrosc.* **1997**, *28*, 697.

(29) Gu, X. J. *J. Raman Spectrosc.* **1996**, *27*, 83.

(30) Pushkarev, V. V.; Kovalchuk, V. I.; d'Itri, J. L. *J. Phys. Chem. B* **2005**, *109*, 17386.

(31) Binet, C.; Daturi, M.; Lavalley, J.-C. *Catal. Today* **1999**, *50*, 207.

(32) Takeguchi, T.; Manabe, S.; Kikuchi, R.; Eguchi, K.; Kanazawa, T.; Matsumoto, S.; Ueda, W. *Appl. Catal., A* **2005**, *293*, 91.

(33) Tiernan, M. J.; Finlayson, O. E. *Appl. Catal., B* **1998**, *19*, 23.

(34) Jacobs, G.; Williams, L.; Graham, U.; Sparks, D.; Davis, B. H. *J. Phys. Chem. B* **2003**, *107*, 10398.

(35) Blaser, U.; Jalett, H. 'P.; Montid. M. *Appl. Catal.* **1989**, *52*, 19.

(36) Parka, S. H.; Tzou, M. S.; Sachtler, W. M. H. *Appl. Catal.* **1986**, *24*, 85.

(37) Cotton, F. A.; Wilkinson, G.; Murillo, C. A.; Bochmann, M. *Advanced Inorganic Chemistry*, 6th ed.; Wiley: New York, 1999.

(38) Nakamoto, K. *Infrared and Raman Spectra of Inorganic and Coordination Compounds*, 4th ed.; Wiley: New York, 1986.

(39) Nagai, Y.; Hirabayashi, T.; Dohmae, K.; Takagi, N.; Minami, T.; Shinjoh, H.; Matsumoto, S. *J. Catal.* **2006**, *242*, 103.

(40) Vishwanathan, V.; Narayanan, S. *Catal. Lett.* **1993**, *21*, 183.

(41) Holmgren, A.; Andersson, B. *J. Catal.* **1998**, *178*, 14.